Desalination and Water Treatment
www.deswater.com

doi: 10.1080/19443994.2015.1056834

57 (2016) 13318–13333
June

Taylor & Francis
Taylor & Francis Group

Adsorption of congo red from aqueous solution using various TiO_2 nanoparticles

T. Şişmanoğlu[a,*], G.S. Pozan[b]

[a]*Engineering Faculty, Department of Chemistry, Istanbul University, Istanbul 34320, Turkey, Tel. +90 212 4737070; Fax: +90 212 4737180; email: tusase3@gmail.com*
[b]*Engineering Faculty, Department of Chemical Engineering, Istanbul University, Istanbul 34320, Turkey, Tel. +90 212 4737070; Fax: +90 212 4737180; email: gsdpozan@gmail.com*

Received 21 July 2014; Accepted 24 May 2015

ABSTRACT

In this work, TiO_2 nanopowder (TIP600) was prepared by a sol–gel method and titanium isopropoxide, glacial acetic acid, and deionized water were used as the starting materials. Adsorption of congo red (CR) on Degussa-P25 (P25), commercial TiO_2 (C-TiO_2), and TIP600 was investigated. But, photochemical and photocatalytic event were not used for this adsorption process. Adsorption of CR onto the adsorbents was studied at different temperatures (25.0, 40.0, and 50.0˚C) and various adsorbent doses (0.1, 0.05, and 0.025 g). The kinetics of dye adsorption has been investigated in terms of pseudo-first order, pseudo-second order, and intra-particle diffusion rate. The results indicate that pseudo-second order plays a significant role in the adsorption mechanism. The adsorptive capacity of TIP600 is much higher than that of other adsorbents. The value of $\Delta H^{\#}$ was obtained as positive, therefore the nature of adsorption was found endothermic. Equilibrium isotherm of CR was fitted to the Freundlich and Langmuir models. The equilibrium data of adsorbate were found to best fit the Langmuir model. For CR, TIP-600 was demonstrated as the best adsorption capacity (q_{max} 112 mg g^{-1}).

Keywords: TiO_2 nanopowder; Congo red; Adsorption; Kinetic study; Isotherms

1. Introduction

Dyes and pigments are common constituents of effluents discharged by various industries, particularly in the textile industries. Low concentration of the dye solutions can be highly toxic for water and soil systems. A number of technologies have been developed and used for the removal of the dye pollutants from wastewater such as adsorption, coagulation, ozonation, membrane filtration, and photocatalytic decolorization [1–5]. Especially, azo dyes have the largest group of synthetic colorants and these colorants are released into the environment. Congo red (CR) (3,3´-[[1,1´ biphenyl]-4,4´diylbis-(azo)] bis [4-amino-1-naphthalene-sulfonic acid] disodium salt) is a sulfonated azo dye. It is a water-soluble secondary azo dye and contains an azo (–N=N–) chromophore and an acidic auxochrome (sulfanate-SO_3H) associated with the benzene structure. It is used to dye textiles. Yet, CR is reported to be carcinogenic and highly toxic to living beings. Therefore, this pollutant has to be removed from textile wastewater [6]. Activated carbon was generally used for removal of dyes, because of its excellent adsorption ability [7,8]. However, regeneration process of activated carbon is

*Corresponding author.

highly difficult and uneconomic. Therefore, researchers have attempted to find inexpensive alternative adsorbents. Some natural low-cost adsorbents have been tested for the removal of CR as clay materials, pine [9–11]. Clay minerals are natural hydrophilic compounds, therefore, they are unsuitable and are regarded as adsorbents for organic compounds. However, exchange of inorganic cations of clay minerals with organic cations renders organophilic adsorbents known as organoclay. In addition, modifications are used to increase the surface area [12,13]. However, this procedure is time consuming and it is not economical Also, adsorption of CR was investigated on natural adsorbents such as seeds [14,15].

On the other hand, mesoporous films of a semiconductor oxide can be constituted by a network of nanocrystalline particles such as titanium dioxide and zinc oxide. The choice of oxide material mesoporous films has generally been TiO_2. Its properties are linked to the material content, chemical composition, structure, surface morphology, non-toxicity, and low cost.

In recent years, degradation of CR under UV–light has been examined using photocatalyst or photoactive. Generally, in these studies, nano-TiO_2, ZnO, and nanocomposites are used [16–20]. The sol–gel method [21,22] is widely employed for the preparation of nanoparticles, due to the inexpensive equipment required and the low temperatures involved. However, because of increasing interest in the application of nanosize TiO_2 in different fields, the vast body of literature on titanium deal with the synthesis, properties, and applications of different nanosize titanium crystalline forms; anatase, rutile, and brookite [23–25]. Recently, various nanostructured TiO_2 catalysts have been prepared by hydrolysis of titanium isopropoxide or titanium tetrachloride [26]. The samples derived from $TiCl_4$ were the most active and neither filtration nor calcination was needed to obtain a highly efficient anatase phase. The preparation of nanostructured TiO_2 photocatalysts using $TiCl_4$ as the precursor appears worthy of attention since this compound does not give rise to formation of organic impurities in the final products. The reported other synthesis methods for preparation of titanium nanoparticles, like hydrothermal, solvothermal, and emulsion precipitation [27–29], all face the problem of either poor crystalline form of anatase or broad size distribution [30].

In this study, anastase TiO_2 nanoparticle (TIP600) was synthesized by sol–gel method in short time. Degussa P-25 (P25), commercial TiO_2 (C-TiO_2), and titanium isopropoxide 600˚C (TIP600) were characterized with a number of methods including BET, SEM, XRD, and FTIR. In this paper, adsorption of CR from aqueous solution on Degussa P-25 (P25), C-TiO_2, and TIP600 was especially investigated without any photochemical and photocatalytic event and was not used UV-visible light. The influence of the experimental parameters was studied in terms of contact time and adsorbent dose. For kinetic evaluation, the adsorption process was studied at 25.0, 40.0, and 50.0˚C and the thermodynamic parameters were determined. In addition, adsorption isotherm data were interpreted by the Freundlich and Langmuir equations. The constants of equations were determined and isotherm types were found at constant temperature.

2. Materials and methods

2.1. Adsorbate

CR ($C_{32}H_{22}N_6Na_2O_6S_2$ FW = 696.7 g mol^{-1}, λ_{max} = 510 nm) used in this study as an anionic diazo direct dye was purchased by Sigma Chemical Company. Its chemical structure is shown in Fig. 1. First, the stock solution of CR was prepared in the concentration of 100 mg L^{-1}. Then, this solution was diluted from 1 to 75 mg L^{-1}.

2.2. Adsorbent

Titanium isopropoxide (≥99%, Fluka), Degussa P-25 (consisting of 70% anatase and 30% rutile with a specific BET surface area of 50 m^2/g and primary particle size of 32 nm), and anatase TiO_2 (purity > 99.99%, Aldrich), were purchased and used in their commercial form without any purification.

2.2.1. Preparation of TIP600

TiO_2 nanopowder (TIP600) was prepared by a sol–gel method and titanium isopropoxide, glacial acetic acid, and deionized water were used as the starting materials. The titanium isopropoxide, glacial acetic acid, and water were maintained at the molar ratio of 1:10:350. During the experimental process, titanium isopropoxide was added in glacial acetic acid by vigorous stirring. After obtaining a transparent sol, the

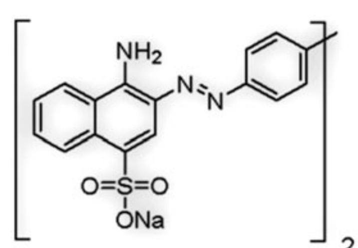

Fig. 1. Structure of congo red (CR).

mixture was aged for 1 h at room temperature and dried at 70°C for one day. Finally, the dried gel was calcined in air at 600°C for 4 h.

2.3. Characterization

Phase identification of the products was carried out by X-ray diffraction (Rigaku D/Max-2200/PC diffractometer with the CuKα ($\lambda = 1.540$) radiation). Samples were scanned from 10° to 80° at a rate of 2°/min. The sizes of the crystalline domains were calculated by using the Scherrer equation,

$$t = C\lambda / B \cos \Theta$$

where λ is the X-ray wavelength (Å), B is the full width at half maximum, Θ is Bragg angle, C is a factor depending on crystallite shape (taken to be one), and t is the crystallite size (Å). Spectroscopic analysis of the nanoparticle TiO_2 samples was performed using a Fourier transform infrared (FT-IR) spectrometer (Perkin Elmer Precisely Spectrum One), and UV–visible spectrophotometer (CHE-BIOS Optimum). The morphology of the products was examined by scanning electron microscopy (JEOL/JSM-6335F).

The specific surface area of the samples was determined through nitrogen adsorption using a surface area analyzer (Quantachrome Inst. 3.12). The samples were degassed at 200°C prior to measurements.

2.4. Experimental procedure

Batch adsorption experiments were carried out using P25, C-TiO_2, and TIP600 as the adsorbent. CR stock solution 100 mg L^{-1} was used and a predetermined doses of the adsorbents (0.1, 0.05, and 0.025 g) were placed in the thermostat at predetermined temperature (25, 40, and 50°C). Samples were taken from this adsorption system after 30 min and were centrifuged for 10 min at constant string speed of 4,000 rpm. The pH value of CR solution on TiO_2 nanoparticles was measured as 8.72 and the concentrations of CR solution at this pH were determined by UV–visible spectrophotometer. All the

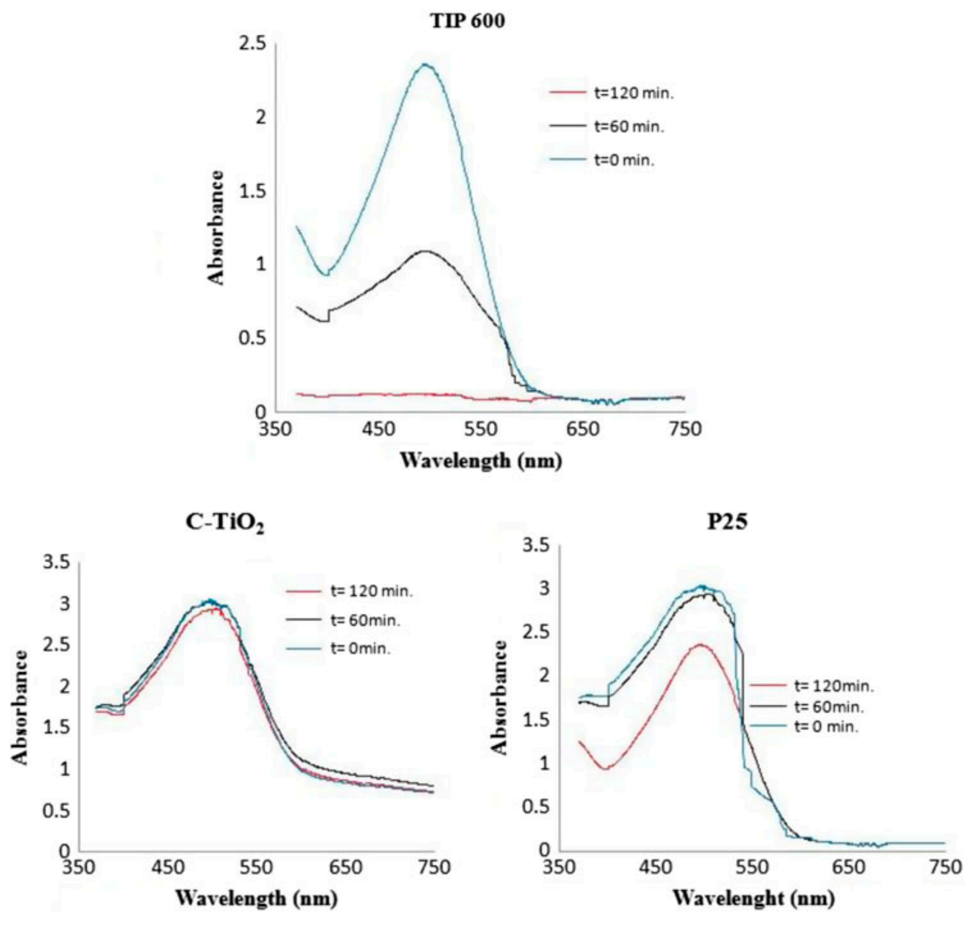

Fig. 2. Adsorption of congo red (100 mg L^{-1}) UV–visible absorption spectra change at different time intervals.

spectrophotometric measurements were made with a CHE-BIOS Optimum UV–visible spectrophotometer. For P25, C-TiO_2, TIP600, UV–visible absorption spectra of aqueous solution of CR (100 mg L^{-1}) were shown in Fig. 2. The maximum absorbance value of CR was measured at 510 nm. The calibration graph of absorbance vs. concentration followed a linear Lambert–Beer relationship [31]. The color removal efficiency of the dye was calculated as the following Eq. (1),

$$\text{Removal efficiency} \quad (\%) = (C_0 - C_t)/C_0 \times 100 \tag{1}$$

where C_0 and C_t are the initial concentration and the concentrations of the dye at any time (mg L^{-1}), respectively. The amount of dye adsorbed per gram of TiO_2 (mg g^{-1}) at any time q_t was calculated by a mass balance relationship Eq. (2).

$$q_t = (C_0 - C_t)\, V/W \tag{2}$$

where V indicates the volume of dye solution (L) and W is the weight of the adsorbent (g).

For each temperature, equilibrium of adsorption has been reached at 180 min as shown in Fig. 3. Rapid process has been occurred until 60 min and then this process has been slowly followed until 130 min. For C-TiO_2 and P25, value concentration of CR has not changed with different adsorbent doses at 50.0℃ as seen in Fig. 3. Plots of concentration of congo vs. time have been the same at 25.0 and 40.0℃. For TIP 600, the concentration of CR has decreased. Its value has changed with increase in the amount of TIP600 at 50.0℃ as seen in Fig. 3. Plots of concentration of congo vs. time have been the same at 25.0 and 40.0℃. Kinetics of adsorption was determined by measuring adsorptive uptake of dye from aqueous solution at different time intervals every 15 min. The amount of dye adsorbed at any time was calculated from the concentration changes during adsorption process according to Eq. (2).

3. Results and discussion

3.1. Effect of adsorbent dose

The effect of the adsorbent dose was studied by keeping the ratio (W/V) 2.5–10 g L^{-1} in Eq. (2) at different temperatures. For all experiments, initial concentration of CR was fixed at 100 mg L^{-1}. For C-TiO_2 and P25, the values removal percentages have not

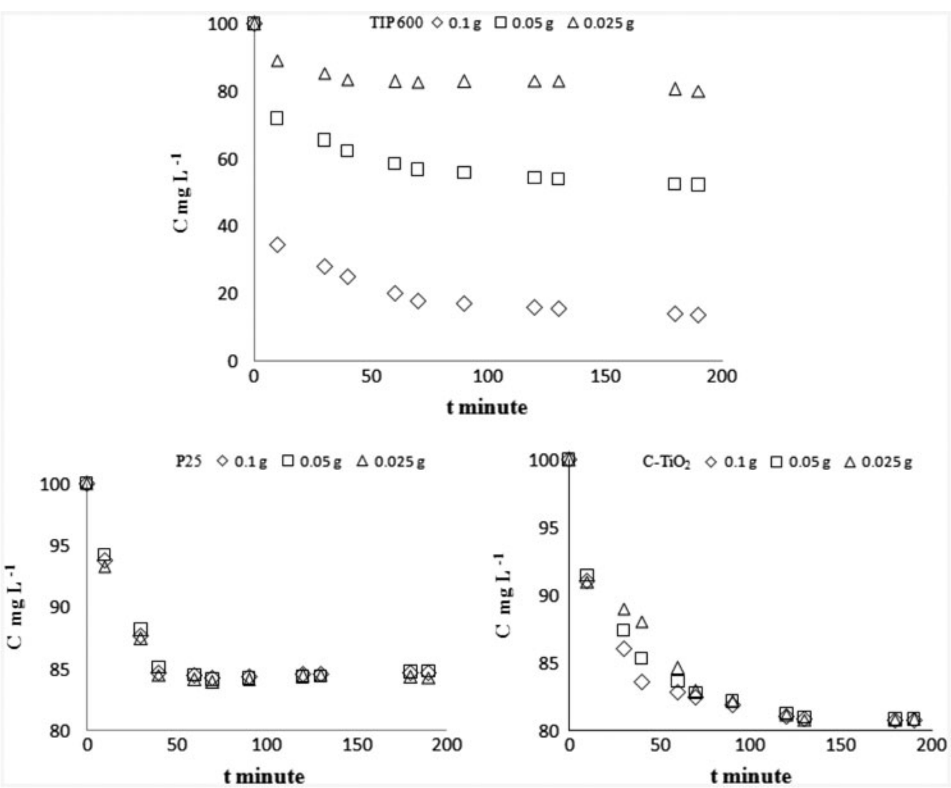

Fig. 3. Plots of concentration of CR vs. time using different adsorbents and doses at 50℃.

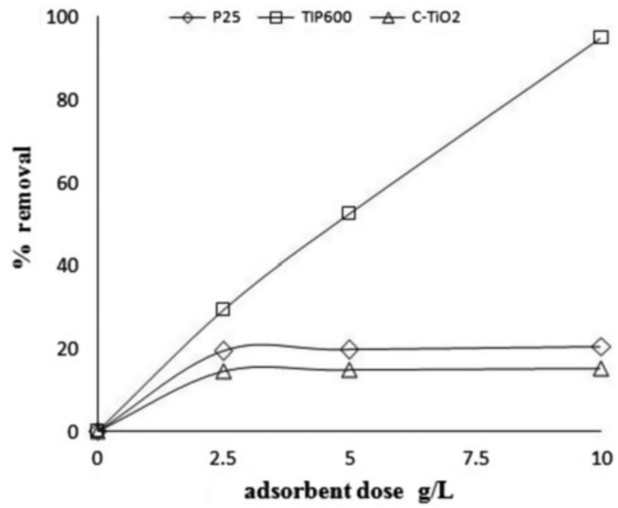

Fig. 4. Effect of adsorbent dose at 50˚C.

changed much with the effect of adsorbent doses at 50˚C, as seen in Fig. 4. For each adsorbent, plots of percent of removal vs. adsorbent doses were similar at 25.0 and 40.0˚C. However, the values removal percentages of CR were increased rapidly with increase in the doses of TIP600 at 50.0˚C as shown in Fig. 4. Plots of percent of removal vs. adsorbent doses were similar at 25.0 and 40.0˚C. Also, values of effect of adsorbent doses are compatible with Fig. 3.

During the adsorption process, the changing of color of CR depending on time and dose is shown in Fig. 5(a) and (b). Except for TIP600, the color of CR is removed using the same proportion for the dose of each adsorbent P25 and C-TiO_2. For TIP600, the maximum amount of CR removal was obtained at the adsorbent dose of 0.1 g. In addition, the color change of the dye onto TIP600 adsorbent is obtained together with other adsorbents.

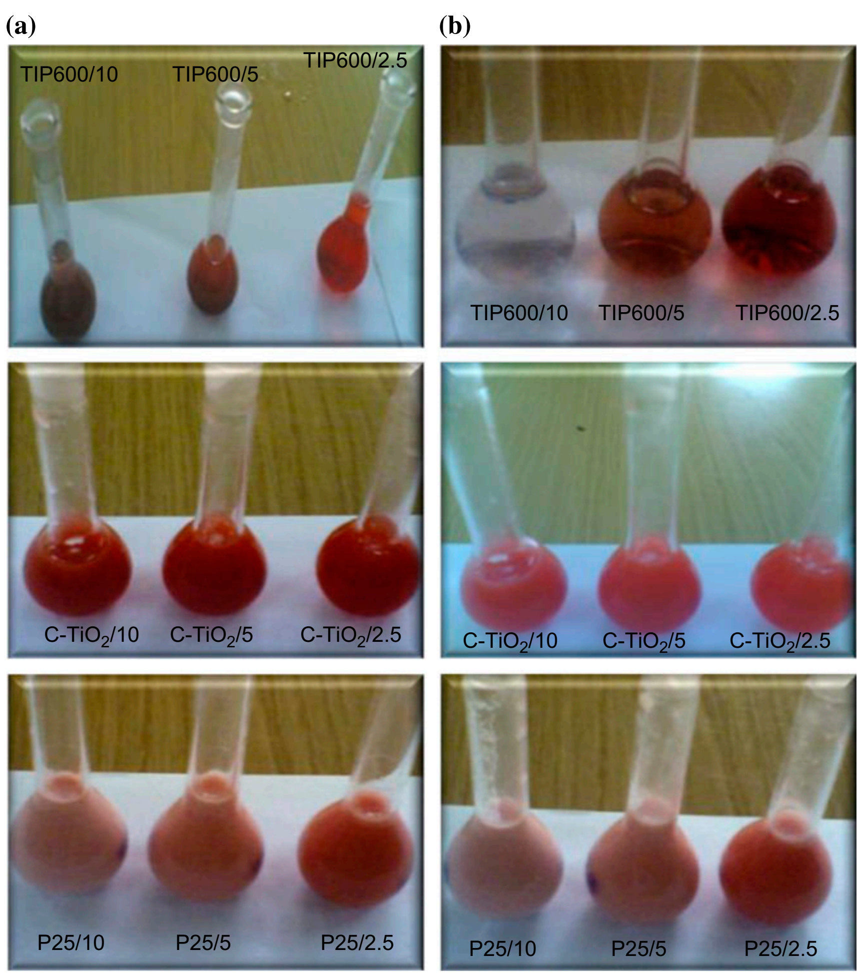

Fig. 5. Color change of congo red (100 mg L^{-1}) by depending adsorbent dose (a) before adsorption and (b) after adsorption.

3.2. Effect of contact time

For three adsorbent doses, the adsorption studies were carried out at different time intervals (from 10 to 180 min) and at different temperatures (25.0, 40.0, and 50.0˚C). For each temperatures and adsorbent doses, the maximum efficiency of P25 and C-TiO_2 was found at 60 and 130 min. The values removal percentages of CR were similar at different temperatures and different adsorbent doses, as seen in Figs. 6A and 6B. The removal percentage of CR was arrived up to 20% within 60 min and this value was not changed in 130 min. Therefore, it can be concluded that the rate of CR binding with adsorbent was great in the initial stages, then gradually decreased and remained almost constant after period. For TIP600 at 0.1 g, the values removal percentages of CR were determined at different temperatures within 60 and 130 min as 85–95%, respectively, as shown in Fig. 7. These values changed at different temperatures for 0.05 and 0.025 g adsorbent doses as 40 and 20%, respectively, as seen in Fig. 7. As shown in Fig. 7, both the instant utilization of the most readily available adsorbing sites on the adsorbent surface and migration of CR from the liquid phase on the TiO_2 nanoparticles surface occured [32]. As a result, adsorption amount of percentage of CR on TIP600 at 50.0˚C is greater than other temperatures.

3.3. BET surface area

The BET surface areas of the adsorbents are measured and the results are listed in Table 1. BET surface areas of adsorbents were measured and found to be as follows: Degussa P-25 (50 $m^2 g^{-1}$) > TiO_2 (TIP600) (45 $m^2 g^{-1}$) > C-TiO_2 (12 $m^2 g^{-1}$). Although surface area of Degussa P-25 was slightly higher than TiO_2 (TIP600), it did not show higher adsorption capacity as shown in Table 1. Particularly, after adsorption, BET surface area of TiO_2 (TIP600) was decreased to 13 $m^2 g^{-1}$. The large decrease in surface area was observed for TIP600 companying to Degussa P-25. This suggests that large CR dye molecules have been adsorbed on the surface of TiO_2 nanoparticles. Adsorbing larger molecules on small particle sizes, adsorbents allow them to be thermally desorbed more easily. This effect may be attributed to the presence of CR molecules in the pore mouths of the TiO_2 channels and pores [33]. The profound effect of adsorbents for CR adsorption is generally considered due to the small crystallite sizes and high anatase phase content.

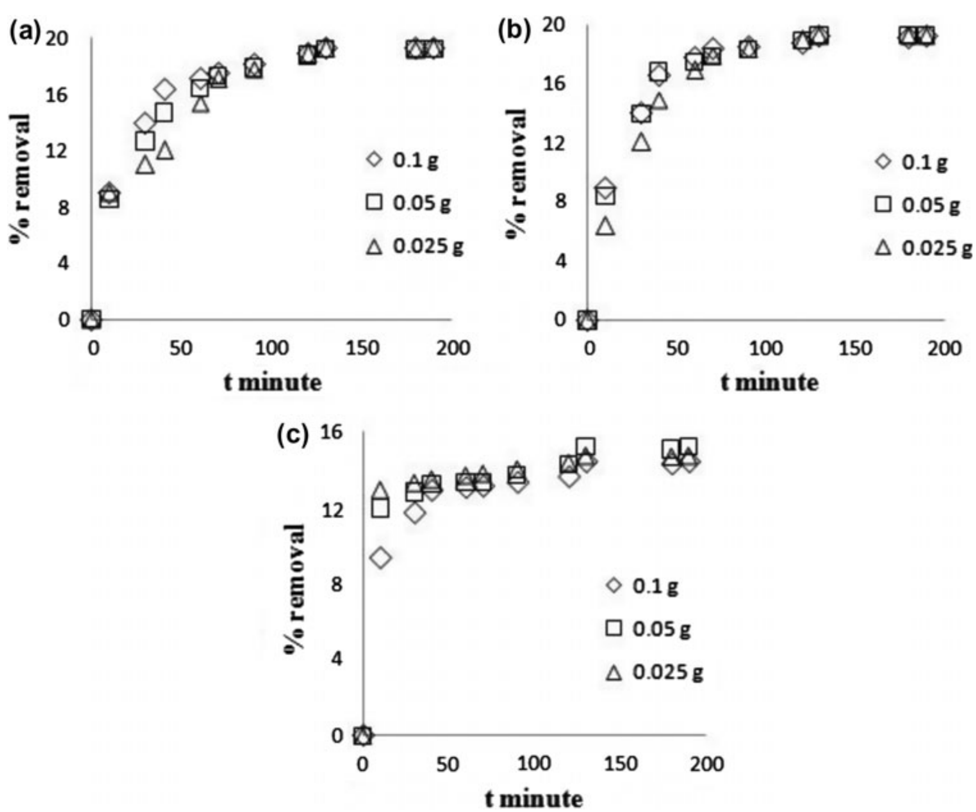

Fig. 6A. Effect of contact time by C-TiO_2 (a) 25.0˚C, (b) 40.0˚C, and (c) 50.0˚C.

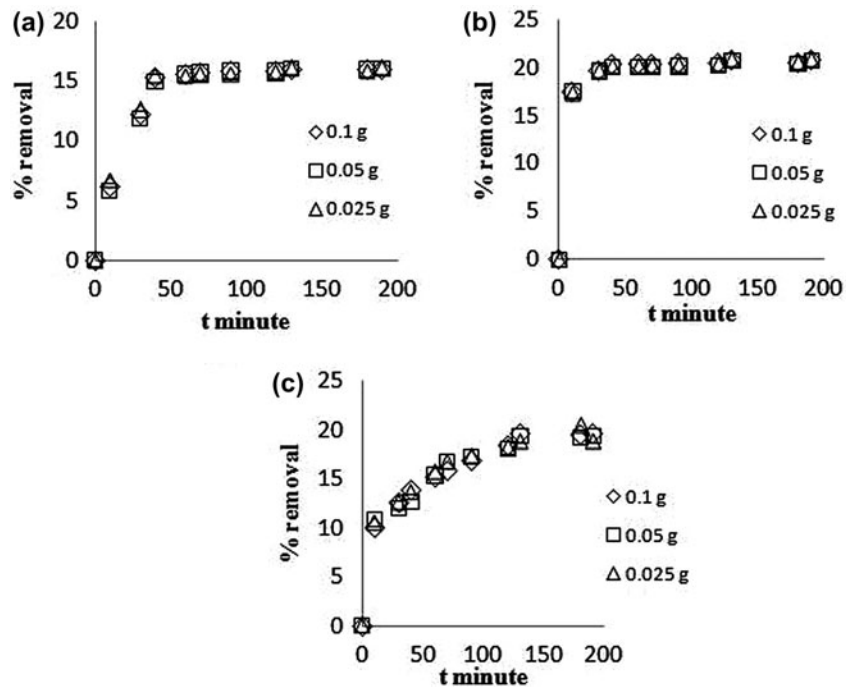

Fig. 6B. Effect of contact time by P25 (a) 25.0˚C, (b) 40.0˚C, and (c) 50.0˚C.

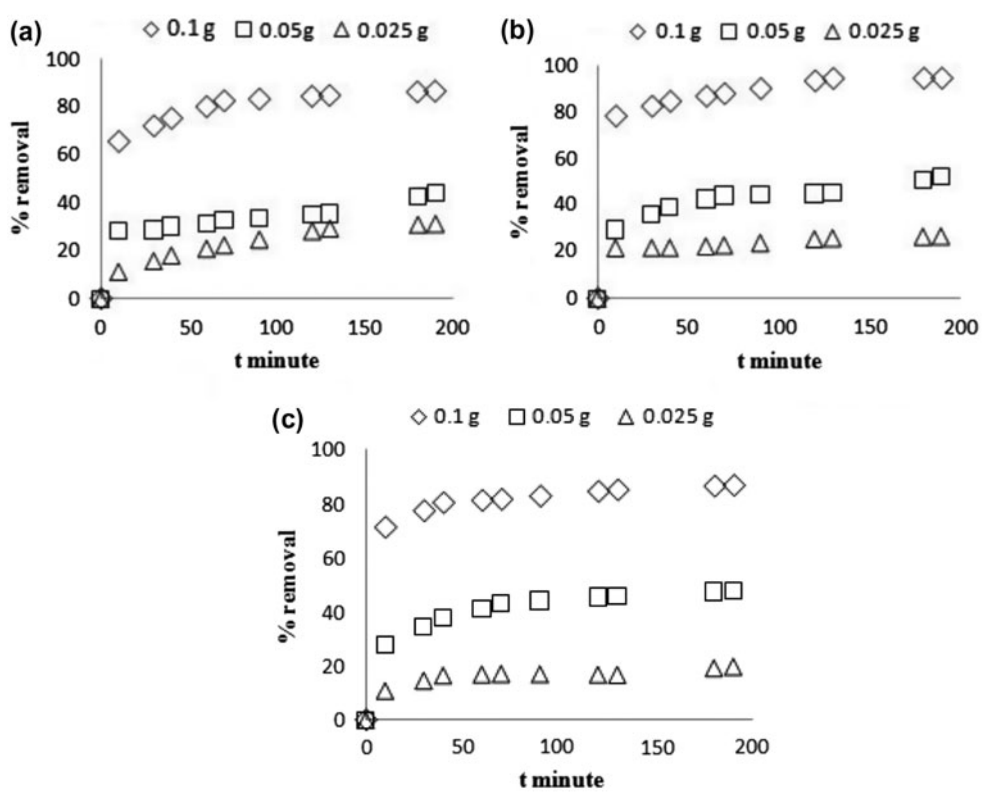

Fig. 7. Effect of contact time by TIP-600 (a) 25.0˚C, (b) 40.0˚C, and (c) 50.0˚C.

Table 1
The crystallite sizes and specific surface areas of adsorbents

Adsorbents	Crystallite size (nm)	S_{BET} (m^2g^{-1})	Morphology
TiO_2 (TIP600)	23	45 (before adsorption) 13 (after adsorption)	100% anatase
C-TiO_2	41	12 (before adsorption) 7 (after adsorption)	100% anatase
Degussa P-25	32	50 (before adsorption) 38 (after adsorption)	70% anatase + 30% rutile

3.4. FTIR measurements

CR has specific peaks in fingerprint region, such as naphthalene and benzene rings. For FTIR spectra of CR, the peaks observed aromatic rings, C=C vibration symmetric stretching of S=O, and asymmetric stretching of S=O, respectively, at the 1,630, 1,280, and 1,155 cm^{-1}. 1,046 and 1,180 cm^{-1} indicate the formation of linkage between SO_3 Na^+ groups and amino groups on the CR molecule. For adsorbents, 3,400 cm^{-1} indicates the stretching modes of O–H bonds of surface-absorbed water. 1,600 cm^{-1} shows that the peaks are the bending vibration of H–O–H bonds from the chemisorbed water, as seen in Fig. 8. It indicates the existence of water on the surface of TiO_2 nanoparticle. After the adsorption of dye, the IR spectra between 1,650 and 1,000 cm^{-1} have been changed for P25, TIP600 and C-TiO_2 nanoparticles. Intensity of adsorption band at 1,600 cm^{-1} increases after adsorption of CR on P25, while the intensity of this band is especially reduced at TIP600 nanoparticle. It clearly indicates that the presence of the water content in the P25 is more than TIP600. So, the amount of adsorption of CR on TIP600 is very high compared to other adsorbents, as seen in Table 2. For C-TiO_2, the bending vibration of H–O–H bonds at 1,600 cm^{-1} is smaller than the bending vibration of H–O–H bonds for P25 but the amount of adsorption of CR on C-TiO_2 is quite low compared to TIP600 adsorbent as seen in Table 2.

3.5. XRD measurements

The X-ray diffractograms of Degussa P-25, C-TiO_2, and TIP600 powders are shown in (Fig. 9). XRD patterns exhibit broad reflections of adsorbents at 25.10, 37.30, 48.10, 53.58, 55.60, and 63.90 Å. In XRD patterns, the diffraction pattern of anatase TiO_2 (JCPDS 21-1272) and rutile TiO_2 (JCPDS 21-1276) was detected. The peaks of the C-TiO_2 are narrow and at low intensity indicates little degree of crystallinity with an anatase phase ($2\theta = 25.10°$). For TIP600, the crystallinity of the anatase phase increased, as shown by the narrower peaks and higher peak intensity Fig. 9. Also, intensity of degree of crystallinity with anatase phases ($2\theta = 37.30°$ and $48.10°$) was increased for TIP600. The rutile peak at $2\theta = 27.6°$, $42.15°$, and $56.10°$ were analyzed for P25. The crystallite sizes (particle size) of the adsorbents are calculated according to the Scherrer formula and the results were listed in Table 1. As shown in Table 1, small particles were formed in the structure of TIP600. It can be concluded that the active site is higher with smaller particles.

3.6. SEM measurements

The SEM photomicrographs of adsorbents (before and after adsorption with CR) are shown in Figs. 10–12, respectively. The TiO_2 spherical nanoparticles are well distributed and it has a porous structure in which the nanoparticles are all bonded together through a sintering process, as seen in Figs. 10(a)–12(a). It was observed in the SEM images that CR molecules were entered into the TiO_2 particles after adsorption of P25 and C-TiO_2. In addition, the particle size was increased, but the surface area was decreased as seen in Table 1. However, after dye adsorption, a significant change was observed in the structure of TIP600 (Fig. 11(b)). Unlike other adsorbents, the surface of TIP600 was completely covered by the CR molecules which entered the spaces between the pores. These are in good agreement with XRD and BET results.

3.7. Kinetic study

In order to investigate the controlling mechanism of adsorption processes such as the pseudo-first order, pseudo-second order, and intra-particle diffusion equations were applied to model the kinetic models of CR adsorption onto nanoparticle P25, TIP600, and C-TiO_2 at three temperatures.

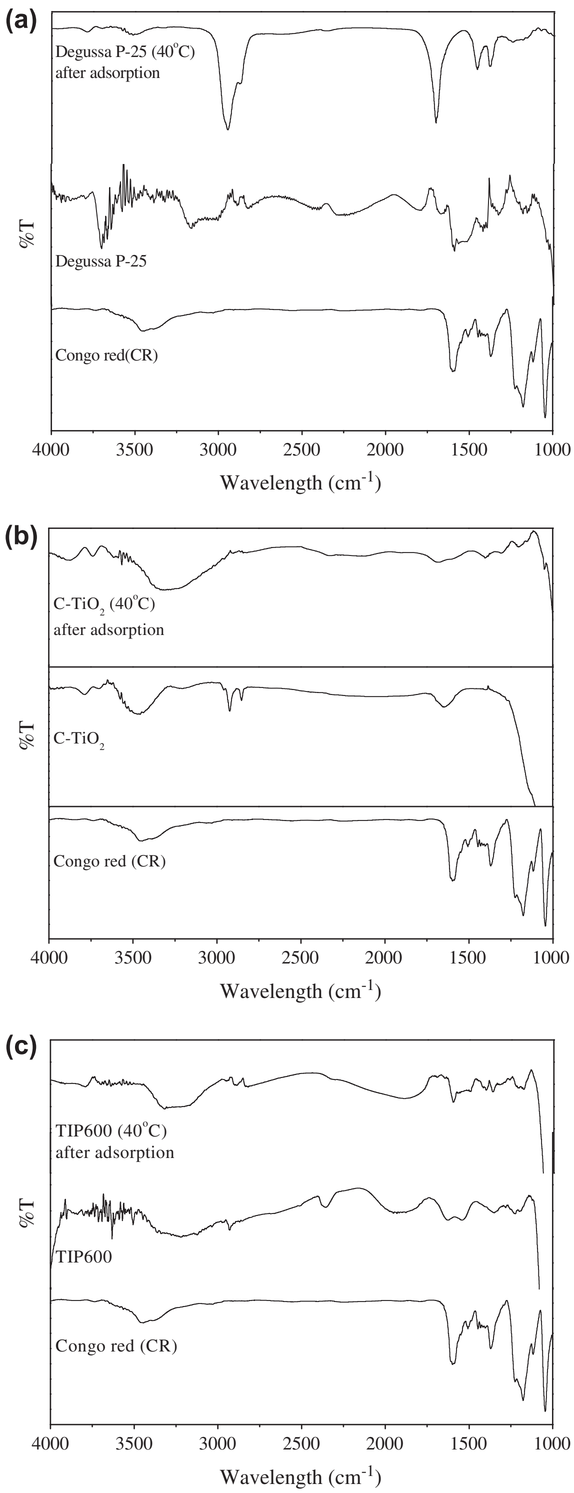

Fig. 8. FTIR spectra of TiO_2 nanoparticles and congo red.

The pseudo-first-order rate equation is given as Eq. (3),

$$\ln(q_e - q_t) = \ln q_e - k_1 t \quad (3)$$

where q_e and q_t are the amounts of dye adsorbed on adsorbent at equilibrium and at any time t, respectively (mg g^{-1}), k_1 is the rate constant of pseudo-first-order model (min^{-1}) [34]. The slope of $\ln(q_e - q_t)$ vs. t was used to determine the rate constant, k_1 and correlation coefficients, R^2.

The pseudo-second-order equation is expressed as Eq. (4) [35],

$$\frac{t}{q_t} = \frac{1}{k_2 q_e^2} + \frac{t}{q_e} \quad (4)$$

$$h = k_2 q_e^2$$

where h is the initial adsorption rate (mg g^{-1} min^{-1}).

The plot t/q_t vs. t should give a straight line if pseudo-second-order kinetics is applicable and q_e, k_2, and h can be determined from the slope and intercept of the plot, respectively.

The intra-particle diffusion is estimated by the following Eq. (5) [36],

$$q_t = k_i t^{1/2} + c \quad (5)$$

where k_i is the initial rate of sorption controlled by intra-particle diffusion (mg g^{-1} $min^{-1/2}$). The plot of q_t vs.$t^{1/2}$ should give a linear relationship and k_i can be determined from the slope of the plot.

The data obtained from adsorption of CR does not fit with the pseudo-first-order equation because the values of correlation coefficients of this equation are less $R^2 < 0.98$ as given in Table 2. The best fit was found on the pseudo-second-order model. Both the rate constants of pseudo-first order and intra-particle diffusion changed irregularly with increasing temperature, but the rate constant of pseudo-second order increased with increasing temperature, as seen in Table 2. It was observed that both the calculation ($q_{e,cal}$) and experimental ($q_{e,exp.}$) findings were compatible with each other. For adsorbent dose 0.1 g of TIP600 at 50°C temperature, the amount of dye adsorbed at equilibrium (q_e) was calculated as the highest value compared to q_e values of other adsorbents.

From the plots of q_t vs. $t^{1/2}$ of CR, two-step linear lines were observed in Table 2. While the first step shows the diffusion of CR through the solution to the external surface of TiO_2 nanoparticles, the second step suggests the gradual adsorption. [37]. The regression coefficient values suggest that the adsorption of adsorbate varies almost linearly with the half power of time ($t^{1/2}$) as given in Table 2.

Table 2
Kinetic parameters for the adsorption of congo red onto the nanoparticle TiO_2

Adsorbent/dose (g)	P25/0.1			P25/0.05			P25/0.025			TIP600/0.1			TIP600/0.05			TIP600/0.025			C-TiO_2/0.1			C-TiO_2/0.05			C-TiO_2/0.025		
t (ºC)	25	40	50	25	40	50	25	40	50	25	40	50	25	40	50	25	40	50	25	40	50	25	40	50	25	40	50
$q_{e,exp}{}^{a}$	16.2	19.6	20.8	16.1	19.3	20.8	16.0	18.8	20.7	86.5	86.7	94.8	52.1	52.4	59.5	19.9	26.8	29.3	19.2	19.3	14.4	19.1	19.3	15.1	19.2	19.3	14.7
$q_{e,cal}{}^{a}$	7.81	1.89	12.3	8.18	1.86	11.8	4.97	2.1	12.6	15.4	25	25	23	21	51	6.43	7.4	23.5	12.3	10.0	4.08	14.5	11.2	3.41	19.9	18.3	2.21
$k_{11}{}^{b} \times 10^2$	2.2	1.6	2.2	2.0	1.1	1.0	0.9	1.2	1.8	2.9	2.9	1.5	2.8	2.8	1.0	3.1	3.4	1.3	4.1	1.8	1.8	3.8	1.3	1.8	2.6	1.5	2.4
R^2	0.86	0.64	0.98	0.85	0.64	0.96	0.65	0.68	0.98	0.97	0.96	0.92	0.98	0.97	0.86	0.60	0.82	0.38	0.97	0.92	0.84	0.97	0.96	0.95	0.96	0.98	0.97
$q_{e,cal}{}^{a}$	18.5	20.4	21	18	20	20.8	17.6	20	20.8	90	91	100	50	50	59	18.2	26.4	32.1	21.2	21.2	14.3	21.7	21	14.5	22.7	21.8	14.5
$k_2{}^{c} \times 10^2$	0.3	0.42	3.4	0.28	0.35	4.0	0.32	0.53	3.2	0.2	0.22	0.24	0.08	0.18	0.24	0.01	0.63	1.1	0.35	0.38	1.3	0.25	0.34	1.8	0.17	0.19	2.6
R^2	0.99	1.0	1.0	0.99	1.0	1.0	0.99	1.0	1.0	0.99	1.0	1.0	0.99	0.99	1.0	0.99	1.0	1.0	0.99	0.99	1.0	0.99	0.99	1.0	0.97	0.99	1.0
$k_{i1}{}^{d}$	2.82	0.93	1.07	2.82	0.82	1.06	2.71	0.92	1.06	2.6	2.9	1.9	2.4	3.1	2.1	0.75	0.04	2.05	2.3	2.35	0.51	1.9	2.61	0.27	1.42	2.63	0.18
$k_{i2}{}^{d}$	0.09	0.03	–	0.08	0.04	–	0.05	0.06	–	–	1.05	–	–	–	–	–	0.95	–	0.54	0.25	–	0.68	0.42	–	–	0.57	–
R^2	0.99	0.99	0.99	0.99	0.98	0.94	0.99	0.99	0.98	0.95	0.99	0.99	0.95	0.96	0.92	0.71	0.99	0.98	0.99	0.99	0.80	0.99	0.99	0.96	0.95	0.99	0.99
	–	0.60	–	0.82	0.98	–	0.98	0.98	–	–	0.99	–	–	–	–	–	0.98	–	0.99	0.95	–	0.96	0.99	–	–	0.89	–

Note: a = (mg g^{-1}), b = (min^{-1}), c = (g mg^{-1} min^{-1}), and d = (mg g^{-1} $min^{-1/2}$).

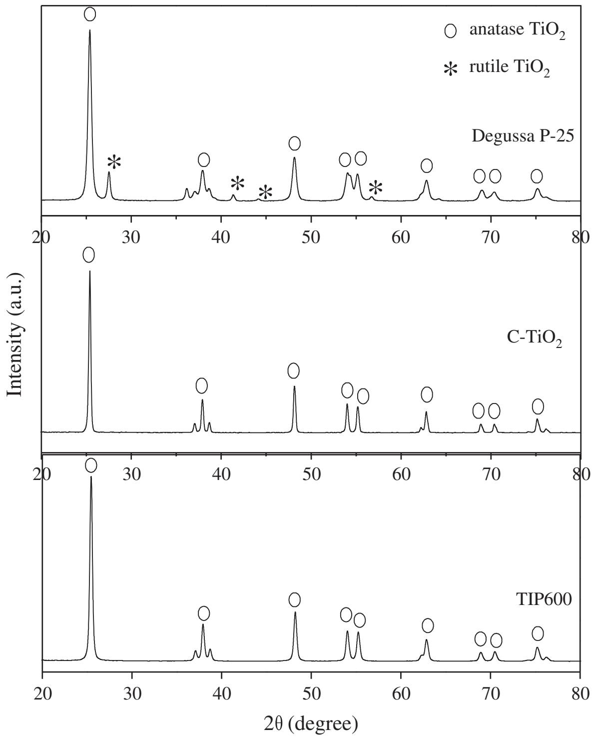

Fig. 9. Powder X-ray diffraction patterns of adsorbents.

3.8. Thermodynamic parameters

From the rate constant k_2 (Table 2), the activation energy E_a for the adsorption of CR on P25, TIP600, and C-TiO_2 was determined using the Arrhenius Eq. (6).

$$\ln k = \ln A - \frac{E_a}{RT} \quad (6)$$

where E_a, R, and A refer to the Arrhenius activation energy, the gas constant, and Arrhenius factor, respectively.

The enthalpy $\Delta H^{\#}$, entropy $\Delta S^{\#}$ were calculated using the Eyring Eq. (7).

$$\ln \frac{k}{T} = \ln \frac{k_b}{h} + \frac{\Delta S^{\#}}{R} - \frac{\Delta H^{\#}}{RT} \quad (7)$$

where k_b and h refer to Boltzmann's constant and Planck's constant, respectively [38]. The free energy of activation $\Delta G^{\#}$ was obtained from equation ($\Delta G^{\#} = \Delta H^{\#} - \Delta S^{\#}$). The calculated values obtained from pseudo-second-order model are listed in Table 3. Because the value of the activation energy E_a was between 5.8 and 79 kJ mol^{-1}, the adsorption mechanism was physical adsorption as seen in Table 3. The negative value of the activation entropy $\Delta S^{\#}$ has shown the interaction between CR and the adsorbents. The positive values of $\Delta G^{\#}$ and $\Delta H^{\#}$ indicate that the adsorption process is non-spontaneous in nature and support an endothermic reaction.

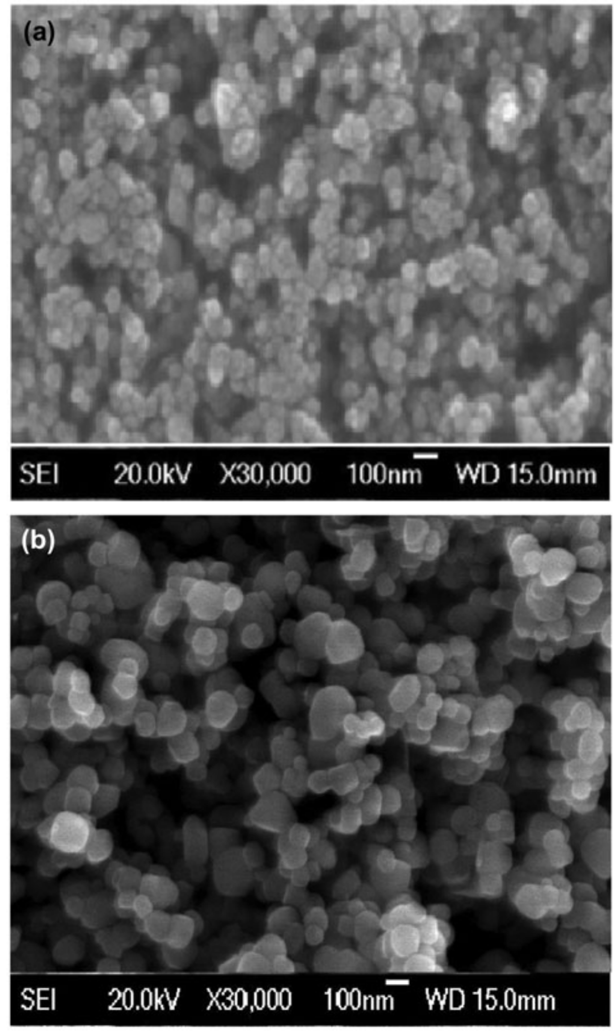

Fig. 10. SEM images of P25 (a) before adsorption of dye and (b) after adsorption of dye.

3.9. Adsorption isotherms

According to the classification of Giles et al. [39], the shape of isotherms was obtained for CR on the adsorbents C-TiO_2, P25, and TIP600 L-type ($n \leq 1$) at 50 ℃. When longitudinal axis of adsorbed molecules is parallel to the adsorbent surface, L-shaped isotherms are obtained as seen in Fig. 13 [40].

The adsorption data fitted both Langmuir and Freundlich isotherms for CR adsorbed on the titanium oxide nanoparticle adsorbents.

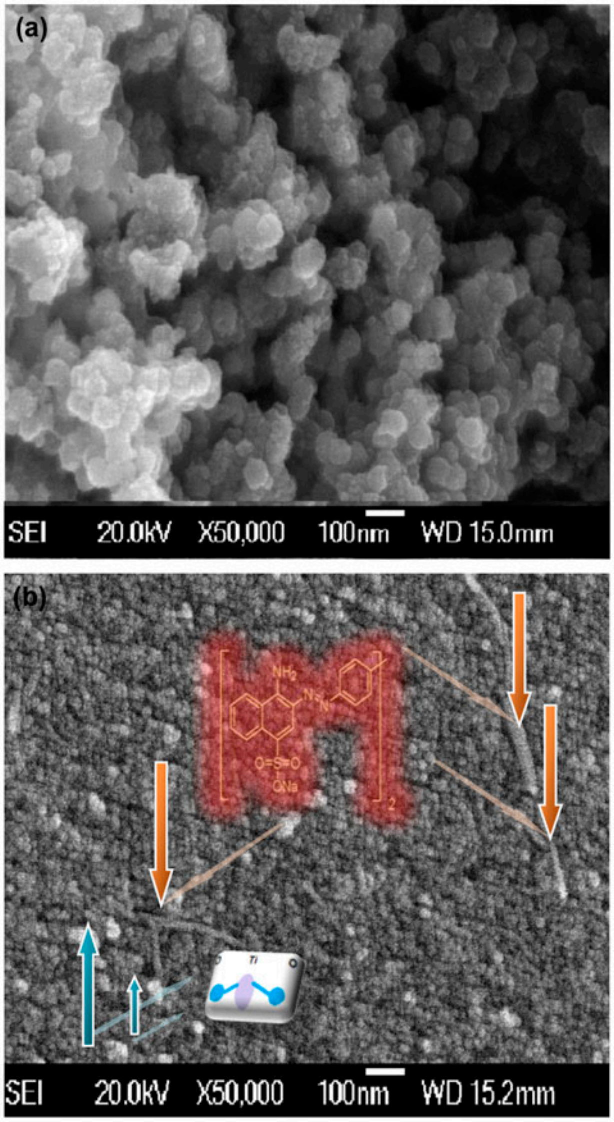

Fig. 11. SEM images of TIP600 (a) before adsorption of dye and (b) after adsorption of dye.

The Langmuir isotherm is shown in Eq. (8) as follows:

$$\frac{1}{q_e} = \frac{1}{q_{\max}} + \frac{1}{q_{\max}\, b\, c_e} \quad (8)$$

where $q_{\max}$ is the maximum adsorption capacity that corresponds to complete monolayer coverage (mg g^{-1}), b is the adsorption equilibrium constant (L mg^{-1}). When $1/q_e$ is plotted against $1/c_e$, a straight line with slope b and intercept $1/q_{\max}$ is obtained. This graph shows that the adsorption obeys Langmuir isotherm model for TIP600 as seen in Fig. 14.

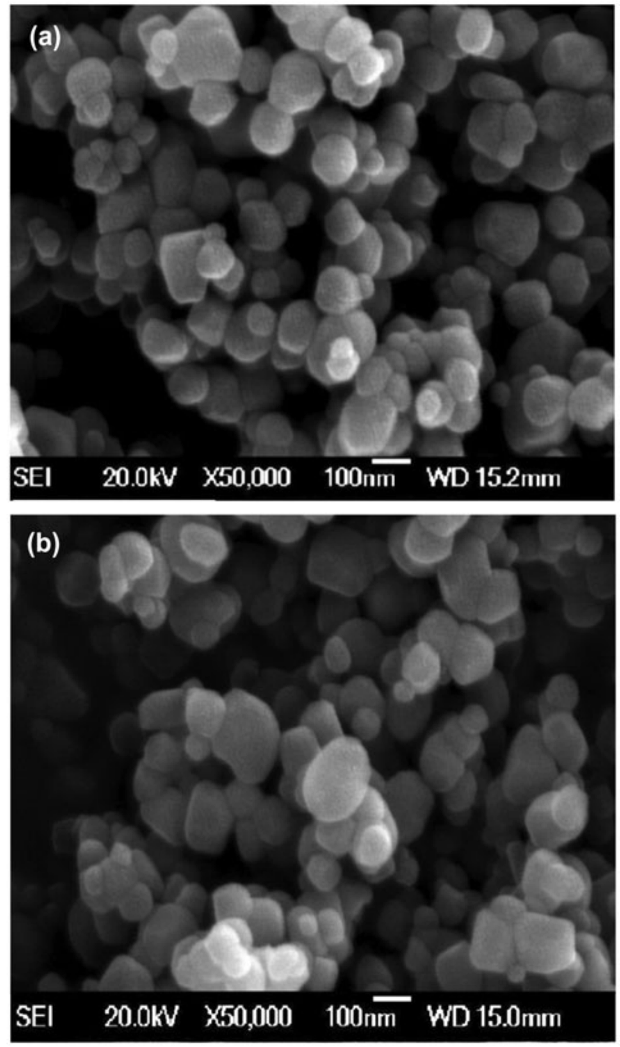

Fig. 12. SEM images of C-TiO_2 (a) before adsorption of dye and (b) after adsorption of dye.

The Freundlich model is shown in Eq. (9) as follows:

$$q_e = K_f\, c_e^n \quad (9)$$

where K_f and n are the Freundlich constants that quantify the adsorption capacity and adsorption intensity, respectively. The values of K_f and n are determined from the intercept and slope of the linear regressions. The slope n should have values in the range of 0 to1 for favorable adsorption [41]. As indicated in Table 4, the dye is favorable adsorption on the magnitude of Freundlich constant for each adsorbent, as seen in Fig. 15.

The isotherm constants obtained from linearized Langmuir and Freundlich isotherm equations are

Table 3
Thermodynamic parameters for the adsorption of congo red onto the nanoparticle TiO_2

Adsorbent/dose (g)	E_a (kj mol^{-1}) (25–50℃)	$\Delta H^{\#}$ (kj mol^{-1}) (25–50℃)	$\Delta S^{\#}$ (j mol^{-1} K^{-1}) (25–50℃)	$\Delta G^{\#}$ (kj mol^{-1}) (25℃)
P25/0.1	72	69	−62.3	88
P25/0.05	78	76	−43.5	89
P25/0.025	69	67	−71	88
TIP600/0.1	5.8	3.2	−286	89
TIP600/0.05	46	43	−152	88
TIP600/0.025	36	33	−192	90
C-TiO_2/0.1	38	36	−173	88
C-TiO_2/0.05	59	56	−108	88
C-TiO_2/0.025	79	77	−44	90

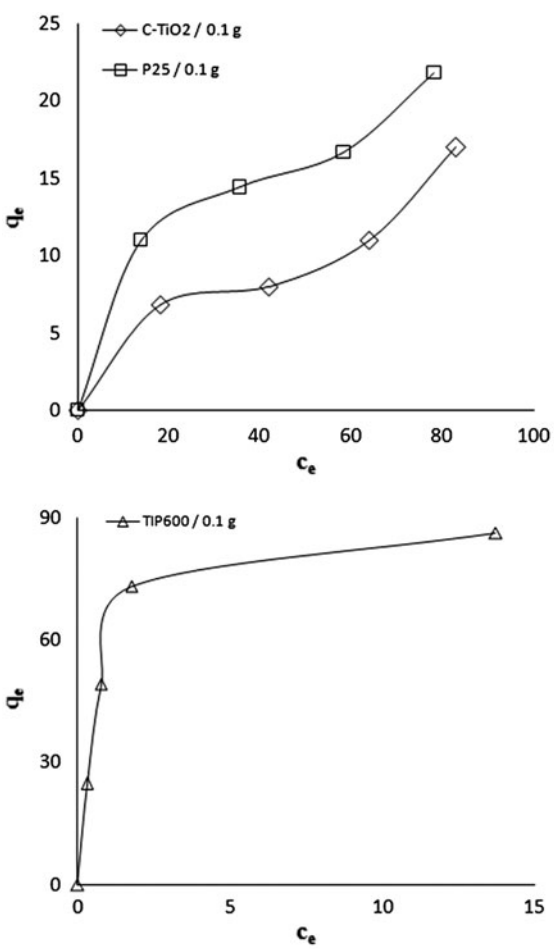

Fig. 13. Isotherm type of congo red on adsorbents at 50.0℃.

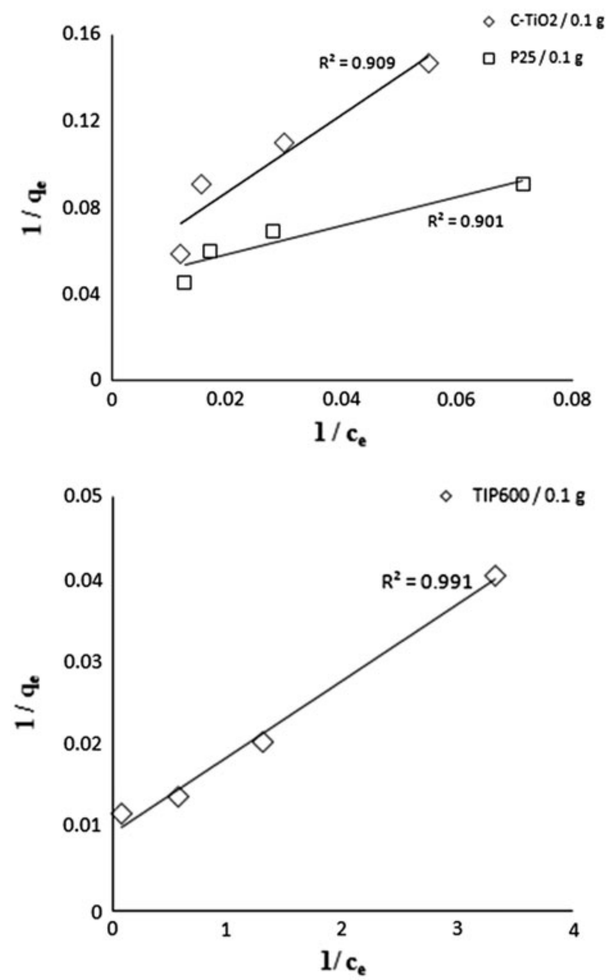

Fig. 14. Langmuir isotherm of congo red on adsorbents at 50.0℃.

given in Table 4. The correlation coefficient for CR adsorbent on TIP600 obtained from Langmuir isotherm were found $R = 0.99$, 0.99, 0.98 for the adsorbent of 0.1–0.05–0.025 g, respectively, and for Freundlich expression these values were found $R = 0.80$, 0.87, 0.86, respectively. However, for 0.1–0.05–0.025 g Degussa P-25 and C-TiO_2 the correlation coefficient

Table 4
Adsorption isotherm constants for the adsorption of congo red onto the nanoparticle TiO_2 at 50°C

Isotherms/adsorbent	P25/0.1	P25/0.05	P25/0.025	TIP600/0.1	TIP600/0.05	TIP600/0.025	$C\text{-}TiO_2/0.1$	$C\text{-}TiO_2/0.05$	$C\text{-}TiO_2/0.025$
Freundlich									
n	0.4	0.3	0.3	0.3	0.3	0.3	0.5	0.8	0.6
K_f	4.0	4.6	5.2	46.2	17.6	5.7	1.3	0.4	1.4
R	0.98	0.94	0.95	0.80	0.87	0.86	0.81	0.83	0.87
Langmuir									
q_{max}	22.7	21.3	20.0	112	53	26	20	19.6	18.9
$b \times 10^{-3}$	66	75	87	1000	310	98	28	16	31
R	0.91	0.95	0.97	0.99	0.99	0.98	0.92	0.76	0.85

Note: $q_{max} = mg\ g^{-1}$.

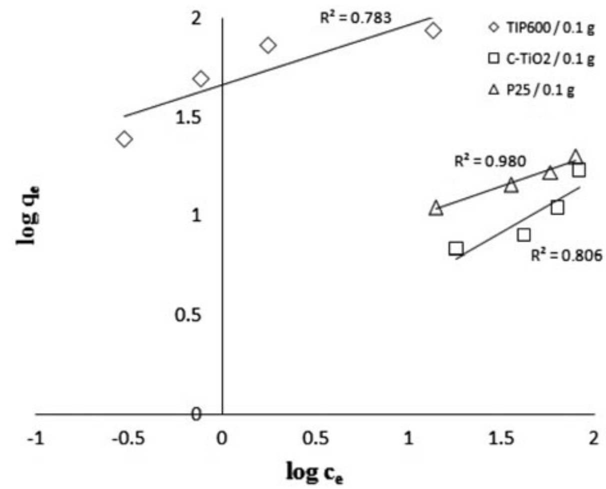

Fig. 15. Freundlich isotherm of congo red on adsorbents at 50.0°C.

were calculated from Langmuir $R = 0.91$, 0.95, 0.97, and $R = 0.92$, 0.76, 0.85, respectively, and from Freundlich expression these were $R = 0.98$, 0.94, 0.95, and $R = 0.81$, 0.83, 0.87, respectively.

The values indicate that Langmuir expression provides better fit with the experimental data of the adsorption of CR on TIP600 than P25 and $C\text{-}TiO_2$. For each adsorbate dose of P25 and $C\text{-}TiO_2$, the values of q_{max} were changed from 18.9 to 22.7 mg g^{-1}as seen in Table 4. Especially, q_{max} value of adsorbate dose 0.1 g for TIP600 is maximum (112 mg g^{-1}) and this value is compatible with q_e value of TIP600 at 50°C as seen in Table 2. All the adsorbents have formed *L*-type isotherm for adsorption of CR. The curvature shows a fairly rapid rise up to saturation and then it becomes increasingly difficult for a solute molecule to find a vacant site available.

4. Conclusions

The results of this study show that TIP600 prepared by sol–gel method have been very effective for the adsorption of CR when compared to other adsorbents. At the wavelength 510 nm, the destruction of chromophore group was disappeared at 120 min during adsorption of CR on TIP 600. For P25 and $C\text{-}TiO_2$, this chromophore group was still seen after 120 min. This indicates that the CR molecule had entered into $C\text{-}TiO_2$ and P25. For this reason, CR adsorption capacity has been due to the blocking effect of the P25 and $C\text{-}TiO_2$ pore system.

For the adsorption process of CR, kinetic studies were conducted and thermodynamic parameters were also calculated. The best fit was obtained for the pseudo-second-order model. For the adsorbent dose of 0.1 g, the values of the amounts of dye on the adsorbents at equilibrium at 50°C temperature were calculated to be as TIP600 (100 mg g^{-1}) > P25 (21 mg g^{-1}) > C-TiO_2 (14.3 mg g^{-1}). The adsorption mechanism was physical adsorption, because of the value of E_a between 5.8 and 79 kJ mol^{-1}. The negative value of the activation entropy $\Delta S^{\#}$ has shown the interaction between CR and the adsorbents used in this study. The highest negative value of the activation entropy was obtained with 0.1 g adsorbent dose of TIP600. Therefore, adsorption capacity of TIP600 for CR removal shows a promise for the potential applications.

The adsorption isotherm for the CR adsorbed on the titanium oxide nanoparticle adsorbents was fitted to the Langmuir and Freundlich isotherms. The results indicate that Langmuir expression provided better fit for the experimental data of CR on TIP600 than on P25 and C-TiO_2. The value of q_{max} at the adsorbate dose of 0.1 g is maximum (112 mg g^{-1}) for TIP600 and this value is compatible with q_e value of TIP600 at 50°C.

As a result, TIP600 nanoparticle was synthesized via sol–gel method in short time and the adsorption capacity was found to be higher than other adsorbents used in this study.

Acknowledgments

This study was supported by the Scientific Research Project Fund of Istanbul University, project no: 12671. The author would like to thank Prof.Dr. Ayşe Zehra Aroğuz and associate professor Derya Dışpınar from Istanbul University for the editing of the manuscript in terms of grammar.

References

[1] G.M. Walker, L. Hansen, J.A. Hanna, S.J. Allen, Kinetics of a reactive dye adsorption onto dolomitic sorbents, Water Res. 37 (2003) 2081–2089.

[2] B. Shi, G. Li, D. Wang, C. Feng, H. Tang, Removal of direct dyes by coagulation: The performance of preformed polymeric aluminum species, J. Hazard. Mater. 143(1–2) (2007) 567–574.

[3] A.C. Gomes, J.C. Nunes, R.M.S. Simões, Determination of fast ozone oxidation rate for textile dyes by using a continuous quench-flow system, J. Hazard. Mater. 178 (2010) 57–65.

[4] P. Denyer, L. Shu, V. Jegatheesan, Evidence of changes in membrane pore characteristics due to filtration of dye bath liquors, Desalination 204 (2007) 296–306.

[5] H. Kominami, H. Kumamoto, Y. Kera, B. Ohtani, Photocatalytic decolorization and mineralization of malachite green in an aqueous suspension of titanium (IV) oxide nano-particles under aerated conditions: Correlation between some physical properties and their photocatalytic activity, J. Photochem. Photobiol., A 160 (2003) 99–104.

[6] C.I. Pearce, J.R. Lloyd, J.T. Guthrie, The removal of colour from textile wastewater using whole bacterial cells: A review, Dyes Pigm. 58 (2003) 179–196.

[7] E. Lorenc-Grabowska, G. Gryglewicz, Adsorption characteristics of congo red on coal-based mesoporous activated carbon, Dyes & Pigm. 74 (2007) 34–40.

[8] J. Pal, M. Deb, Efficient adsorption of congo red dye from aqueous solution using green synthesized coinage nanoparticles coated activated carbon beads, Appl. NanoSci. 4(8) (2014) 967–978.

[9] V. Vimonses, S. Lei, B. Jin, C.W.K. Chow, C. Saint, Kinetic study and equilibrium isotherm analysis of congo red adsorption by clay materials, Chem. Eng. J. 148 (2009) 354–364.

[10] S. Dawood, T.K. Sen, Removal of anionic dye congo red from aqueous solution by raw pine and acid-treated pinecone powder as adsorbent: Equilibrium, thermodynamic, kinetics, mechanism and process design, Water Res. 46(6) (2012) 1933–1946.

[11] B. Meroufel, O. Benali, M. Benyahia, Y. Benmoussa, M.A. Zenasni, Adsorptive removal of anionic dye from aqueous solutions by Algerian kaolin: Characteristics, isotherm, kinetic and thermodynamic studies, J. Mater. Environ. Sci. 4(3) (2013) 482–491.

[12] L. Wang, A. Wang, Adsorption properties of Congo Red from aqueous solution onto surfactant-modified montmorillonite, J. Hazard. Mater. 160 (2008) 173–180.

[13] M.A. Zenasni, B. Meroufel, A. Merlin, B. George, Adsorption of congo red from aqueous solution using CTAB-kaolin from Bechar Algeria, J. Surf. Eng. Mater. Adv. Tech. 4 (2014) 332–341.

[14] D.B. Jirekar, M. Farooqui, Adsorption of congo red from aqueous solution using eco-friendly low cost material prepared from *Cicerarientinum*, Arab. J. Phys. Chemis. 2(1) (2015) 1–6.

[15] M.C. Somasekhara Reddy, L. Sivaramakrishna, A. Varada Reddy, The use of an agricultural waste material, Jujuba seeds for the removal of anionic dye (Congo red) from aqueous medium, J. Hazard. Mater. 203–204 (2012) 118–127.

[16] H. Guo, K. Lin, Z. Zheng, F. Xiao, S. Li, Sulfanilic acid-modified P25 TiO_2 nanoparticles with improved photocatalytic degradation on Congo red under visible light, Dyes Pigm. 92 (2012) 1278–1284.

[17] M.N. Chong, S. Lei, B. Jina, C. Saint, C.W.K. Chow, Optimisation of an annular photoreactor process for degradation of Congo Red using a newly synthesized titania impregnated kaolinite nano-photocatalyst, Sep. Purif. Technol. 67 (2009) 355–363.

[18] E. Dvininov, E. Popovici, R. Pode, L. Cocheci, P. Barvinschi, V. Nica, Synthesis and characterization of TiO_2-pillared Romanian clay and their application for azoic dyes photodegradation, J. Hazard. Mater. 167 (2009) 1050–1056.

[19] R. Djellabi, M.F. Ghorab, G. Cerrato, S. Morandi, S. Gatto, V. Oldani, A. Di Michele, C.L. Bianchi, Photoactive TiO_2–montmorillonite composite for degradation of organic dyes in water, J. Photochem. Photobiol., A 295 (2014) 57–63.

[20] N.H.H. Hairom, A.W. Mohammad, A.A.H. Kadhum, Effect of various zinc oxide nanoparticles in membrane photocatalytic reactor for congo red dye treatment, Sep. Purif. Tech. 137 (2014) 74–81.

[21] C.J. Brinker, G.W. Scherer, Sol–Gel Science: The Physics and Chemistry of Sol–Gel Processing, Academic Press, New York, NY, 1990.

[22] D.A. Ward, E.I. Ko, Preparing catalytic materials by the sol-gel method, Ind. Eng. Chem. Res. 34 (1995) 421–433.

[23] N. Uekawa, M. Suzuki, T. Ohmiya, F. Mori, Y.J. Wu, K. Kakegawa, Synthesis of rutile and anatase TiO_2 nanoparticles from Ti-peroxy compound aqueous solution with polyols, J. Mater. Res. 18 (2003) 797–803.

[24] H. Choi, E. Stathatos, D.D. Dionysiou, Synthesis of nanocrystalline photocatalytic TiO_2 thin films and particles using sol–gel method modified with nonionic surfactants, Thin Solid Films 510 (2006) 107–114.

[25] S.J. Lee, C.H. Lee, Fabrication of nano-sized TiO_2 powder via an ethylene glycol entrapment route, Mater. Lett. 56 (2002) 705–708.

[26] M. Addamo, V. Augugliaro, A. Di Paola, E. García-López, V. Loddo, G. Marcì, R. Molinari, L. Palmisano, M. Schiavello, Preparation, characterization, and photoactivity of polycrystalline nanostructured TiO_2 catalysts, J. Phys. Chem. B 108(10) (2004) 3303.

[27] M. Wu, G. Lin, G. Wang, D. He, S. Feng, R. Xu, Sol-hydrothermal synthesis and hydrothermally structural evolution of nanocrystal titaniumdioxide, Chem. Mater. 14(5) (2002) 1974–1980.

[28] C.S. Kim, B.K. Moon, J.H. Park, B.C. Choi, H.J. Seo, Solvothermal synthesis of nanocrystalline TiO_2 in toluene with surfactant, J. Cryst. Growth 257(3–4) (2003) 309–315.

[29] T. Nakashima, N. Kimizuka, Interfacial synthesis of hollow TiO_2 microspheres in ionic liquids, J. Am. Chem. Soc. 125 (2003) 6386–6387.

[30] D. Pan, N. Zhao, Q. Wang, S. Jiang, X. Ji, L. An, Facial synthesis and characterization of luminescent TiO_2 nanocrystals, Adv. Mater. 17 (2005) 1991–1995.

[31] V. Belessi, G. Romanos, N. Boukos, D. Lambropoulou, C. Trapalis, Removal of Reactive Red 195 from aqueous solutions by adsorption on the surface of TiO_2 nanoparticles, J. Hazard. Mater. 170 (2009) 836–844.

[32] P.S. Kumar, K. Kirthika, Equilibrium and kinetic study of adsorption of nickel from aqueous solution onto *Bael Tree Leaf Powder*, J. Eng. Sci. Tech. 4(4) (2009) 351–363.

[33] T.E. Beesley, B. Buglio, R.P.W. Scott, Sample collection, transport and storage, in: Quantitative Chromatographic Analysis, Marcel Dekker, New York, NY, 2001.

[34] T. Sismanoglu, Y. Kismir, S. Karakus, Single and binary adsorption of reactive dyes from aqueous solutions onto clinoptilolite, J. Hazard. Mater. 184 (2010) 164–169.

[35] Y.S. Ho, G. McKay, Pseudo-second order model for sorption processes, Process Biochem. 34 (1999) 451–465.

[36] J.R. Weber, J.C. Morris, Kinetics of adsorption on carbon from solutions, J. Sanit. Eng. Div. Proc. Am. Soc. Civ. Eng. 89 (1963) 31–59.

[37] Y. Kismir, A.Z. Aroguz, Adsorption characteristics of the hazardous dye Brilliant Green on *Saklıkent mud*, Chem. Eng. J. 172 (2011) 199–206.

[38] T. Sismanoglu, S. Pura, Adsorption of aqueous nitrophenols on clinoptilolite, Colloid Surf. A. 180 (2001) 1–6.

[39] C.H. Giles, A.P. D'Silva, I.A. Easton, A general treatment and classification of the solute adsorption isotherm part. II. Experimental interpretation, J.Colloid Interf. Sci. 47(3) (1974) 766–778.

[40] D.M. Nevskaia, A. Guerrero-Ruíz, J.D. López-González, Adsorption of polyoxyethylenic surfactants on quartz, kaolin, and dolomite: A correlation between surfactant structure and solid surface nature, J. Colloid Interf. Sci. 181(2) (1996) 571–580.

[41] B. Armagan, O.M. Ozdemir Turan, Colour removal of reactive dyes from water clinoptilolite, J. Environ. Sci. Heal. A. 39(5) (2004) 1251–1261.